Journal of Applied Polymer Science

Investigation and modelling of damping mechanisms of magnetorheological elastomers

Raa Khimi Shuib,[1,2] Kim Louise Pickering[1]

[1]School of Engineering, The University of Waikato, Hamilton 3216, New Zealand

[2]School of Materials and Mineral Resources Engineering, USM Engineering Campus, Universiti Sains Malaysia, 14300 Nibong Tebal, Penang, Malaysia

Correspondence to: R. K. Shuib (E-mail: raa_khimi@hotmail.com)

ABSTRACT: Damping in MREs is considered to be ascribed to viscous flow of the rubber matrix, interfacial damping at the interface between the magnetic particles and the matrix and magnetism induced damping. In this study, individual components in MREs that contribute to material damping were investigated. A model was developed to include viscous flow of the rubber matrix, interfacial damping and magnetism induced damping to give the total damping capacity of MREs $\psi_{MRE}(\psi_{MRE})$It was found that ψ_{MRE} depends on frequency, iron sand content, strain amplitude and ψ_{MRE} is independent of the applied magnetic field over saturation magnetization. The proposed model was assessed experimentally using a series of isotropic and anisotropic MREs. Comparison between tan δ with ψ_{MRE} showed that ψ_{MRE} matched the experimental trends with average percentage difference of 8.1% and 21.8% for MREs with modified iron sand unmodified iron sand, respectively. © 2015 Wiley Periodicals, Inc. J. Appl. Polym. Sci. **2016**, *133*, 43247.

KEYWORDS: elastomers; properties and characterization; theory and modeling

Received 30 April 2015; accepted 17 November 2015

DOI: 10.1002/app.43247

INTRODUCTION

Magnetorheological elastomers (MREs) are a new group of damping materials which consist of a non-magnetic matrix (normally an elastomer) containing a suspension of magnetically permeable particles. The most commonly used magnetic particles for MREs are carbonyl iron particles and suitable matrix materials include natural rubber, silicone rubber, polybutadiene, polyisobutylene, polyisoprene, and polyurethene rubber.[1–7] These materials promote damping mainly by the viscous flow of the rubber matrix, but inclusion of magnetic particles in rubber enables additional damping through magnetic particle interaction and interfacial damping. Furthermore, damping and stiffness can be controlled by the application of an applied magnetic field during fabrication or in service. MREs can be fabricated to contain a uniform suspension of magnetic particles (isotropic MREs). However, it has been found that when a magnetic field is applied during curing, chain-like structures of magnetic particles are formed within the rubber (anisotropic MREs) which provides much larger damping and stiffness.[2] Over the past few years, MREs have attracted increasing attention and have been considered for applications such as adaptive tuned vibration absorbers,[8] automotive engine mounts[4] and semi active seismic dampers.[9]

At present, numerous models have been developed to investigate the dynamic mechanical properties of MREs.[6,10–15] However, literature on the modelling of MRE damping mechanisms is limited. Early models were developed by Davis[16] and Jolly *et al.*[17] describing the effect of inter-particle magnetic interactions on the elastic properties of MREs, particularly on the shear modulus. Their work was based on prior theoretical and finite element analyses of MRFs. The developed models use assumptions that the particles are spherical and aligned in perfect chains where the quasi-static shear strains and associated stresses are uniformly distributed over the length of each particle chain. These models have the ability to predict shear modulus well. However, prediction of damping was neglected and mechanisms other than inter-particle magnetic interactions were not included. Lin[18] and Yancheng *et al.*[19] proposed interfacial slip models to describe contributions of the interface between magnetic particles and the rubber matrix to damping but not damping mechanisms associated with the matrix and magnetic particle interactions and so these models would be expected to be limited with respect to describing total damping. Furthermore, these models were not verified experimentally.

Chen and Jerrams[20] were the first to try to take account of all damping mechanisms. They proposed a model to predict overall shear modulus of MREs under cyclic deformation from separate

shear moduli representing the different mechanisms, taking into account the viscoelasticity of the rubber matrix, interfacial slippage between magnetic particles and the matrix and inter-particle magnetic interactions. Tan δ was then obtained from the combined shear modulus. The model is suggested to be potentially reliable for prediction of the overall damping for MREs with weakly bonded interfaces between magnetic particles and the matrix, but less accurate for MREs containing surface modified particles with strongly bonded interfaces due to additional energy absorbed during viscous flow which is more constrained due to the formation of interfacial bonding between particles and the matrix and energy loss due to stress released after debonding of particles from the matrix. The effectiveness of the model was tested by numerical simulations, however, the results were not verified experimentally.

More recently, Jie *et al.*[21] developed a model that also aimed to take account of all possible damping mechanisms to predict overall damping of MREs. This took account of intrinsic damping of component materials, interfacial damping and inter-particle magnetic damping. In their model, the rule of mixtures (commonly used to model the strength of unidirectional, continuous fibre composites)[22] was used to describe the intrinsic damping, assuming MREs as particle reinforced composites with magnetic particle chains of infinite length. The contribution to damping for strongly bonded interfaces was proposed based on Eshelby inclusion theory[23] and the contribution for weakly bonded interfaces was proposed based on Coulomb's law of friction.[24] The contribution for inter-particle magnetic damping was described using the inter-particle magnetic interactions model developed by Jolly *et al.*[17] The model has the ability to explain the experimental trends but the differences between predicted damping values and experimental values were more than 40% which is most likely due to over-simplication in prediction of intrinsic damping by using the ROM. Furthermore, the dependence of frequency on material damping was neglected.

The aim of the current work was to accurately predict total damping capacity of MREs and verify the relative important of different damping mechanisms to the total damping capacity of previously developed MREs based on iron sand and natural rubber[25–27] taking account the separate mechanisms that would contribute to damping, namely:

I. Viscous flow of the rubber matrix,
II. Interfacial damping through strongly bonded interfaces and weakly bonded interfaces,
III. Magnetic-induced damping.

The contribution of viscous flow of the rubber matrix on the overall damping was characterised using the Kelvin Voight model.[28] The contribution to damping for strongly bonded interfaces was described using Schoeck theory[29] which is originally based on Eshelby inclusion theory[23] and the contribution for weakly bonded interfaces was proposed based on Lavernia analysis[30] which is based on Coulomb's law of friction.[24] The inter-particle magnetic interactions model developed by Jolly *et al.*[17] was adopted to evaluate the magnetic-induced damping. According to the author's knowledge, no comprehensive work was dedicated to model the total damping capacity of MRE considering individual components (viscous flow of rubber matrix, interfacial damping and magnetism induced damping) in MREs and their contributions to damping. The developed model can serve as a foundation model for different types of MREs that covers all damping mechanisms.

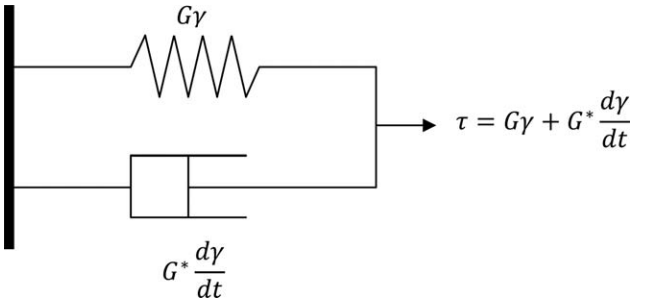

Figure 1. Representation of rubber elastic and viscous components according to the Kelvin Voight model.

THEORETICAL MODELLING

Damping Mechanisms of MREs

Damping in MRE is considered to be mainly by the viscous flow of the rubber matrix and inclusion of magnetic particles enables additional damping through interfacial damping at the interface between the magnetic particles and the matrix and magnetism induced damping. Therefore, modelling of total damping capacity of MREs requires identification of the individual components in the material and a determination of their contributions to the total damping. Thus, the overall damping of MREs taking account the separate mechanisms can be expressed as

$$\psi_{MRE} = \psi_V + \psi_I + \psi_M \tag{1}$$

where ψ_{MRE} is the overall material damping capacity, ψ_V is viscous damping, ψ_I is interface damping and ψ_M is magnetism induced damping.

Viscous Damping

Viscous damping of MREs is mainly provided by the rubber matrix. Rubber is a viscoelastic material which exhibits both viscous and elastic behaviour. The elastic stress follows Hooke's law where stress is directly proportional to strain while the viscous stress follows Newton's law of viscosity, which states that, viscous stress is proportional to strain rate. For a viscoelastic material, the stress–strain relationship is expressed by a linear differential equation with respect to time. A commonly employed relationship is based on the Kelvin Voight model. This model can be represented by spring and dashpost elements (Figure 1) and can be expressed as:

$$\tau = G\gamma + G^* \frac{d\gamma}{dt} \tag{2}$$

In eq. (2), G is shear modulus and G^* is a complex modulus. The term $G\gamma$ represents the elastic component which does not contribute to damping. The term $G^*\ d\gamma/dt$ is the viscous component and embodies for damping. From the Kelvin Voight model, the viscous damping per unit volume is

$$\psi_V = G^* \oint \frac{d\gamma}{dt}\, d\gamma \tag{3}$$

If the material is subjected to a harmonic (sinusoidal) excitation, at steady state, the strain can be expressed as follows

$$\gamma = \gamma_{max} \cos\omega t \tag{4}$$

By substituting eq. (4) into 3, the damping capacity per unit volume can be expressed as

$$\psi_V = \pi\omega G^* \gamma_{max}^2 \tag{5}$$

Now, $\gamma = \gamma_{max}$ when $t = 0$ in eq. (4), or when $d\gamma/dt = 0$. The corresponding stress according to eq. (2), is $\tau_{max} = G\gamma_{max}$. It follows that

$$\psi_V = \frac{\pi\omega G^* \tau_{max}^2}{G^2} \tag{6}$$

so it would be expected that ψ_V depends on the frequency, ω. At low levels of damping (tan $\delta < 1$) for viscoelastic material, ψ_V can be equated with other common damping measures as estimated in references[28,31] and can expressed as follows:

$$\psi_V = \eta = tan\ \delta \tag{7}$$

where η is the loss factor which is defined as the specific damping capacity per radian of damping cycle and tan δ is a comparison between energy lost to that stored; tan δ is obtained by dividing the loss modulus (G'') by the storage modulus (G').[32]

Interfacial Damping

The interface between magnetic particles and the matrix is also important in determining the damping of MREs. Interfacial damping can be attributed to damping through strongly bonded interfaces and weakly bonded interfaces. In the next section the model for damping through strongly bonded interfaces and weakly bonded interfaces are described.

Strongly Bonded Interfaces. For MREs containing particles with functionalized surfaces, polymer molecules can bond to the surface of the particles such that a third phase is formed known as the interphase. The interphase possesses properties distinct from those of the matrix and the particles. The interphase mainly plays the role of transferring stress between the matrix to the reinforced particles. The energy absorption could be attributed to energy required to bring about viscous flow of constrained materials in the vicinity of the particle interfaces, as well as breakdown of interfacial bonding when the applied strain amplitude is high, resulting in transformation of elastic energy into kinetic energy, which then converts into heat. MREs with strongly bonded interfaces can be characterized by Schoeck theory.[29] Based on Schoeck theory, the contribution of interfacial damping of strongly bonded interfaces can be expressed as follows:

$$\psi_I^s = \frac{1}{\tau^2} \frac{1-\vartheta}{3\pi(2-\vartheta)} \frac{1}{V_p} \sum_{i=1}^{n} r_i^3 \left(\tilde{\tau}^2\right)_i \tag{8}$$

where ψ_I^s denotes the strongly bonded interfacial damping, τ is the applied shear stress, ϑ is the Poisson's ratio of the matrix, V_p is volume fraction of the particle, r_i is the radius of the ith particle and $(\tilde{\tau})_i$ is the component of τ in the plane of the ith particle that has relative motion during viscous flow. The following assumption has been made to simplify the calculation; the particles all have the same diameter, the shear stress on each particle is identical and the stress concentration coefficient $\tilde{}_i/\tau$ is taken as 1.5 as in the references.[29,30] Then, the contribution of interfacial damping of strongly bonded interface in MREs can be simplified as

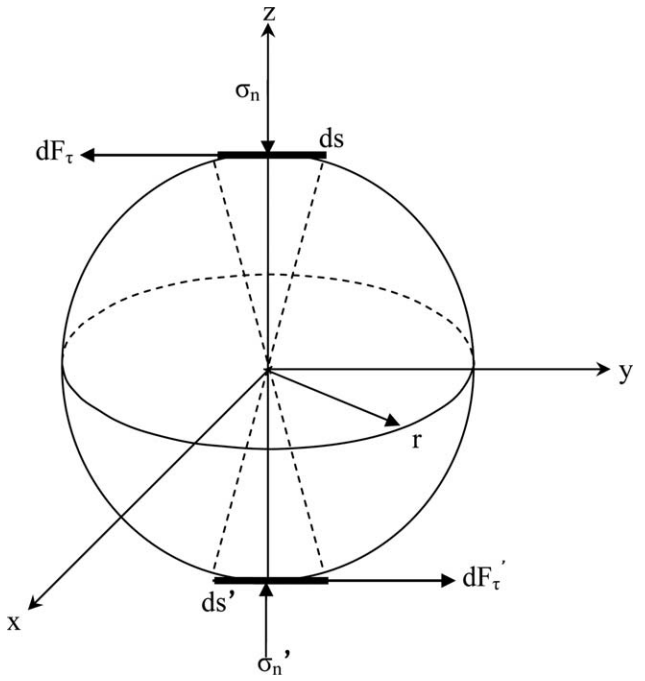

Figure 2. A schematic of the force at the interface where relative movement is likely to occur.

$$\psi_I^s = \frac{4.5\ (1-\vartheta)}{\pi^2(2-\vartheta)} V_p \tag{9}$$

Equation (9) indicates that the damping due to a strongly bonded interface is related to the particle content and the Poisson's ratio of the matrix materials.

Weakly Bonded Interfaces. Weakly bonded interfaces are formed due to weak interactions between particles and the matrix. For weakly bonded interfaces, the damping is mainly due to interfacial friction between the surfaces of particles and the matrix during deformation. The effect of weakly bonded interfaces on the overall damping of the composites can be characterised using Lavernia analysis.[30] In this analysis, the damping is determined by the friction coefficient between the two constituents and the normal stress at the interface where the relative moment is likely to occur as shown in Figure 2.

As shown in Figure 2, the change of area that has relative movement is denoted as ds and the normal stress at ds is denoted as σ_n. When the applied stress is sufficient to overcome the resistance due to friction, relative displacement occurs, $r(\gamma_0\text{-}\gamma_{crt})$, where γ_0 is the corresponding strain amplitude and γ_{crt} is the critical strain of relative movement. The friction on the area ds is given as

$$dF_\tau = (f\sigma_n)ds \tag{10}$$

where f is the friction coefficient for the particle and matrix. Then, corresponding dissipated energy could be written as

$$dU_{dissipation} = r(\gamma_o - \gamma_{crt})(f\sigma_n)ds \tag{11}$$

The dissipation energy per unit volume in the materials over the whole particle surface can be expressed as

$$U_{dissipation} = \frac{\sum_{i=0}^{n} \oint r(\gamma_o - \gamma_{crt})(f\sigma_n)ds}{V} = \frac{3\pi}{4} fV_p\sigma_n(\gamma_o - \gamma_{crt}) \tag{12}$$

where V is volume of the MREs and V_p is the volume fraction of the particles. For simplification, equation $V_p = \frac{1}{V}\sum_{i=0}^{n} V_i$ is utilized where V_i is the volume of ith particle. The elastic energy stored in the material is determined as follows:

$$U_{elastic} = \frac{\frac{1}{2}\tau_o^2}{G} \tag{13}$$

where τ_o is applied stress, G is the shear modulus of the MREs. Subsequently, the damping can be expressed as

$$\psi_I^w = \frac{U_{dissipation}}{U_{elastic}} = \frac{3\pi}{2} \cdot \frac{fV_p\sigma_n(\gamma_o - \gamma_{crt})}{\tau_o^2/G} \tag{14}$$

For a weakly bonded interface, it is assumed that γ_{crt} is much smaller than γ_o and therefore eq. (14) can be written as

$$\psi_I^w = \frac{3\pi}{2} \cdot \frac{fV_p\sigma_n}{\tau_0} \tag{15}$$

As stated in Refs. 33,34, τ_0 can be equated as $\tau_0 = \sigma_{xy}$ where σ_{xy} is effective stress at the particle interfaces in the xy plane (see Figure 2). Then, eq. (15) can be simplified by introducing $K = \sigma_n/\sigma_{xy}$ which represents the normal stress concentration coefficient at the particle interface with relative moment. In addition, the non-uniform strain state throughout the material during deformation caused by relative movement at the interface, only occurs at part of the interface. Taking into account fraction of interface that has relative movement during deformation, a correction factor C can be introduced in eq. (15) as follows:

$$\psi_I^w = \frac{3\pi}{2} \cdot CfV_pK \tag{16}$$

Equation (16) indicates that the damping with weakly bonded interfaces is proportional to the particle content.

The interfacial damping of MREs can be thought as combination of both strongly bonded and weakly bonded interfaces. Therefore the total interfacial damping can be expressed as:

$$\psi_I = \psi_I^s + \psi_I^w = (1-\varphi)\frac{4.5\ (1-\vartheta)}{\pi^2(2-\vartheta)}V_p + \varphi\frac{3\pi}{2} \cdot CfV_pK \tag{17}$$

where φ is the proportion of weakly bonded interface in comparative relation to the total interfacial damping. According to Jie's analysis,[21] φ is given by

$$\varphi = (1-V_p)^{1/3}(1-\gamma)^{1/3} \tag{18}$$

By substituting eq. (18) into eq. (17), the interfacial damping of MREs can be represented by:

$$\psi_I = \frac{4.5\ (1-\vartheta)}{\pi^2(2-\vartheta)}V_p + \left(\frac{3\pi}{2} \cdot CfK - \frac{4.5\ (1-\vartheta)}{\pi^2(2-\vartheta)}\right)\left((1-V_p)^{1/3}(1-\gamma)^{1/3}\right)V_p \tag{19}$$

Equation (19) indicates that the interfacial damping is related to the particle content and applied strain amplitude

Magnetism Induced Damping

Possible magnetism induced damping in MREs is due to energy absorbed to overcome magnetic interaction between neighbouring particles; a process transform elastic energy into magnetic energy and subsequently dissipates by magnetic hysteresis.[3] Other mechanism includes magnetomechanical damping. The process for energy absorption by the magnetomechanical damping is due to change of magnetic domain structure induced by application of stress.[35–37] The energy absorbed through inter-particle magnetic interactions is considered to far outweigh that through magnetomechanical damping as reported elsewhere.[38] Furthermore, the energy losses due to change of the magnetic domain structure is very difficult to directly measured. Therefore, the model is developed on the basis of inter-particle magnetic interactions.

Figure 3 shows schematic diagrams of two adjacent magnetic particles in a chain with the direction of applied magnetic field, $\vec{H}$ and deformation in response to the external shear strain, γ. Magnetic particles are assumed in the model to share the same spherical shape with diameter, d, and initial centre distance between adjacent particles is assumed to be, r_o. The length of the chain is assumed to be infinite. Upon loading with a shear strain perpendicular to $\vec{H}$, the particle chain deviates from the direction of the magnetic field by θ degrees and the inter-particle distance is stretched to r.

The interaction energy of the two adjacent magnetic particles of equal dipole strength $\vec{m}$[17] with north pole of one particle interacting with the south pole of its neighbour can be written as:

$$U_{interaction} = -\frac{\vec{m}^2(1-3cos^2\ \theta)}{4\pi\mu_1\mu_0|r|^3} = -\frac{\vec{m}^2\left(1-3\frac{r_0^2}{r_o^2+\ x^2}\right)}{4\pi\mu_1\mu_0(r_0^2+\ x^2)^{\frac{3}{2}}} \tag{20}$$

where μ_1 is the permeability of the matrix and μ_0 is the permeability of a vacuum. By defining the scalar shear strain as $\gamma = x/r_o$, the dissipation energy due to separation of particles can be expressed as:

$$U_{dissipation} = -\frac{\vec{m}^2(\gamma^2-2)}{4\pi\mu_1\mu_0 r_o^3(\gamma^2+1)^{\frac{5}{2}}} \tag{21}$$

It is assumed that the particles are aligned in long chains and there are only magnetic interactions between adjacent particles within the chain. The total energy dissipation per unit volume associated with the one dimensional shear strain can be calculated by multiplying inter-particle dissipation energy by the volume fraction of the particles and dividing by the total particle volume as follows:

$$U_{dissipation} = \frac{3V_p\vec{m}^2(2-\gamma^2)}{2\pi^2\mu_1\mu_0 d^3 r_o^3(\gamma^2+1)^{\frac{5}{2}}} \tag{22}$$

where V_p is the volume fraction of the particles in the MREs and d is the particle diameter. The elastic energy stored in the material is determined as follows:

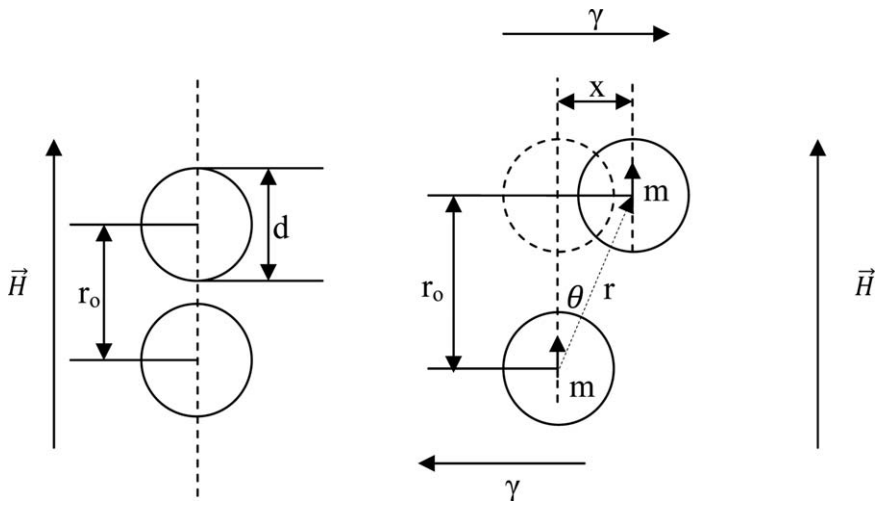

Figure 3. Schematic diagrams of two adjacent magnetic particles in a chain with the direction of applied magnetic field, $\vec{H}$ and deformation of the particle in response to the shear strain, γ.

$$U_{elastic} = \frac{1}{2} G\gamma^2 \tag{23}$$

Subsequently, the magnetic induced damping of MREs can be determined by

$$\psi_M = \frac{U_{dissipation}}{U_{elastic}} = \frac{3V_p\vec{m}^2(2-\gamma^2)}{\pi^2\mu_1\mu_0 d^3 r_o{}^3 G\gamma^2(\gamma^2+1)^{\frac{5}{2}}} \tag{24}$$

As stated in the literature,[17,21] $\vec{m}$ can be defined as $\vec{m}=\frac{1}{6}\pi d^3 J_s$, where J_s is saturation magnetization and $r_o=1.25d$. For iron sand, J_s is estimated to be 0.5 T.[39] Subsequently, the magnetic induced damping of MREs can be rewritten as:

$$\psi_M = \frac{U_{dissipation}}{U_{elastic}} = \frac{0.083V_pJ_s{}^2(2-\gamma^2)}{1.95\mu_1\mu_0 G\gamma^2(\gamma^2+1)^{\frac{5}{2}}} \tag{25}$$

Equation (25) indicates that the magnetic induced damping is related to the particle content, applied strain amplitude and the magnetic induced damping is independent of the applied magnetic field over saturation magnetization.

Overall Damping

From the analysis, the overall damping capacity in MREs containing modified iron sand in natural rubber matrix is derived by substituting eqs. (6), (19) and (25) into eq. (1), as follows:

$$\psi_{MRE} = \frac{\pi\omega G^*\tau_{\max}^2}{G^2} + \frac{4.5\ (1-\vartheta)}{\pi^2(2-\vartheta)}V_p + \left(\frac{3\pi}{2}\cdot CfK - \frac{4.5\ (1-\vartheta)}{\pi^2(2-\vartheta)}\right)\left((1-V_p)^{1/3}(1-\gamma)^{1/3}\right)V_p + \frac{0.083V_pJ_s{}^2(2-\gamma^2)}{1.95\mu_1\mu_0 G\gamma^2(\gamma^2+1)^{\frac{5}{2}}} \tag{26}$$

For MREs containing unmodified iron sand in natural rubber matrix, the contribution of damping through strongly bonded interfaces can be neglected and the overall damping capacity can be derived by modifying eq. (26) and can be can be rewritten as:

$$\psi_{MRE} = \frac{\pi\omega G^*\tau_{\max}^2}{G^2} + \frac{3\pi}{2}\cdot CfV_pK\left((1-V_p)^{1/3}(1-\gamma)^{1/3}\right) + \frac{0.083V_pJ_s{}^2(2-\gamma^2)}{1.95\mu_1\mu_0 G\gamma^2(\gamma^2+1)^{\frac{5}{2}}} \tag{27}$$

Equations (26) and (27) indicates that ψ_{MRE} depends on frequency, iron sand content, strain amplitude and ψ_{MRE} is independent of the applied magnetic field over saturation magnetization.

In this study, G^*, $\tau_{\max}$ and G were obtained from DMA. Poisson's ratio (υ) of rubber is 0.48. The correction factor C has been reported to be 0.5, which assumes 50% of the interface area subjected to the critical strain of relative movement during deformation.[30] The coefficient of friction between iron sand and natural rubber (f) was determined to be 0.21 (the f value was determined according to the procedure as described in reference 41). The stress concentration factor (K) at the interface between iron sand particle and matrix used was 1.2.[30] The relative permeability of a rubber is 1 and the permeability of vacuum is $4\pi\times10^{-7}$ NA^{-2}

EXPERIMENTAL

Materials

Natural rubber (SMR L grade) and other chemicals including zinc oxide, stearic acid, n-cyclohexyl-2-benzothiazole sulfenamide (CBS), tetramethylthiuram disulphide (TMTD), paraffin oil and naphthenic oil were all purchased from Field Rubber Limited, Auckland. Bis-(3-triethoxysilylpropyl) tetrasulphane (TESPT) was purchased from Leap LabChem Co. Limited, China. Iron sand was collected from Ngarunui Beach, Raglan. The iron sand was then milled using a planetary mono mill (Pulverisette 6) produced by Fristech GmbH and subsequently sieved to obtain a 45–56 μm particle size.

Surface Modification of Iron Sand

The surface modification of iron sand was carried out using an aqueous alcohol solution method. Iron sand particles were

Table I. Formulation of Rubber Compounds

Materials	Function	phr*
Natural Rubber	Raw material/matrix	100
ZnO	Activator/peptiser	5
Stearic Acid	Activator/peptiser	1
Paraffin Oil	Plasticiser	2
Naphthenic Oil	Plasticiser	3
Iron sand	Filler	0–70
CBS	Accelerator	2
TMTD	Accelerator	1
Sulphur	Crosslinking agent	1.5
Curing condition	Unit	
Temperature	°C	150
Pressure	Mpa	12
Magnetic field during curing	mT	0–1000

subjected to surface treatment with TESPT at 6 wt % relative to the weight of the particles. An aqueous alcohol solution of 95 vol % ethanol was used and the pH of the solution was adjusted with acetic acid to 4.0–4.5. TESPT of predetermined quantity was dispersed in the ethanol solution at a ratio of 1:100 and the mixed solution was stirred for 5 minutes to ensure hydrolization of the silane coupling agent. The iron sand particles were then added and stirred for an additional 30 minutes at room temperature to ensure a uniform distribution of the coupling agent on the surface of iron sand particles. The mixture was filtered and washed three times with ethanol to remove unreacted coupling agent. The treated iron sand particles were then dried at 80°C in an oven until a constant weight was achieved.

Preparation of Isotropic and Anisotropic MREs

The compound formulation used in this study is given in Table I. Formulations were compounded using a conventional laboratory two roll mill (model XK150) according to ASTM designation D3184-80. The front roller speed was 24 rpm and the rear roller speed was 33 rpm, the roller diameters were 150 mm, friction ratio of two rollers was 1:1.4 and the roller temperature was set to 80°C. The nip gap (distance between front and back roller) was maintained at 2 mm during compounding. The compounding began with softening the rubber on its own in the two roll mill (mastication). Mastication reduces the viscosity and increases the plasticity of natural rubber by mean of heat generated in the two roll mill through conduction from the heated roller and shearing of rubber during milling. After 2–3 minutes the rubber became invested on the hot roll and additives (other than accelerators and sulphur) were then added followed by filler (iron sand or carbon black); addition of accelerators and sulphur were delayed to the last part of the process to prevent premature vulcanization during compounding. The mixing time was approximately 40 minutes. The cure time at 150°C was then determined according to the procedure as described elsewhere.[41] Compounded rubber samples weighing 13g were placed in a mould 60 x 50 x 3 mm. The isotropic MREs and comparative samples were cured in a compression moulder at 150°C under a pressure of approximately 12 MPa. The anisotropic MREs were subjected to an external magnetic field in a specially developed electromagnetic-thermal coupled device (as shown in Figure 4) at 80°C for 30 minutes and subsequently were cured in a compression moulder at 150°C under a pressure of approximately 12 MPa. Finally, post-cure treatment was performed by cooling the anisotropic MREs at room temperature for 30 minutes under an external magnetic field of the same strength as that used during pre-curing. The post-cure treatment was considered necessary to reorientate the magnetic dipoles after compression molding.

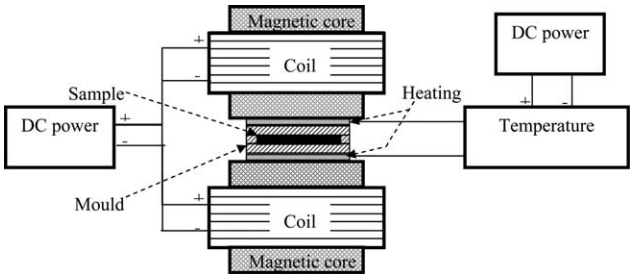

Figure 4. Sketch of specially developed electromagnetic-heat coupled device.

Characterization

Dynamic Mechanical Analysis. Dynamic mechanical analysis (DMA) is a technique used to measure damping of materials as they are deformed under periodic force. In DMA, a sinusoidal force at different frequencies, strain amplitudes and temperatures is applied and displacement of the materials is measured, allowing one to determine the storage modulus (G' or E'), loss modulus (G'' or E'') and tan δ. DMA was carried out using a Perkin Elmer dynamic mechanical analyser (DMA 8000). It is made up of six major components (Figure 5): a force motor, a drive shaft, a high sensitivity displacement detector (LVDT), a sample fixture, a furnace and a temperature controller. The driveshaft motion was kept in a horizontal direction during the test and the temperature controller was placed at a minimum distance from the sample. DMA was carried out using a Perkin Elmer dynamic mechanical analyser (DMA 8000). Tan δ was measured over a series of frequency and strain amplitude ranging from 0.01Hz-130Hz and 0.1–4.5%, respectively. The influence of frequency and strain amplitude on tan δ was assessed

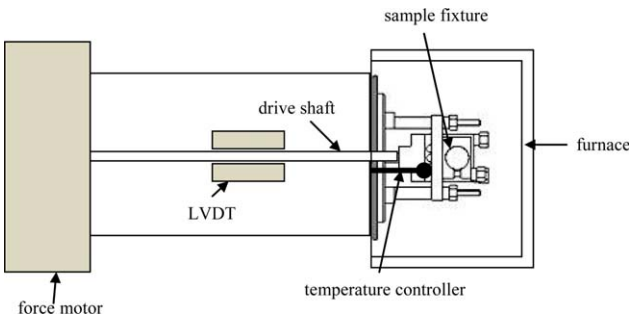

Figure 5. Scheme of the DMA 8000. [Color figure can be viewed in the online issue, which is available at wileyonlinelibrary.com.]

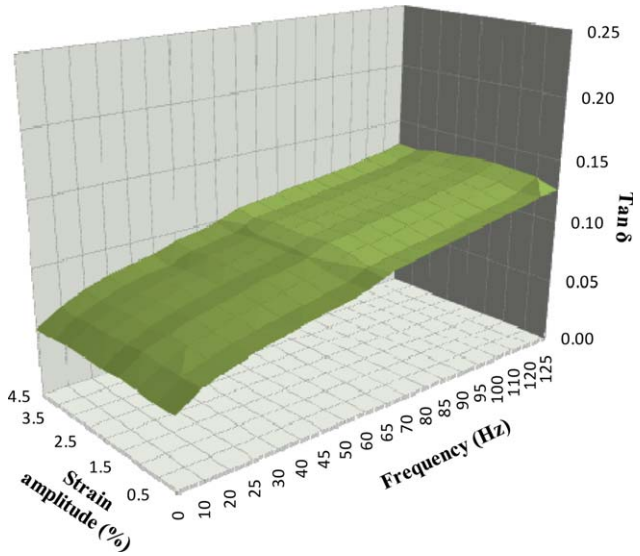

Figure 6. Influence of strain amplitude and frequency on tan δ. [Color figure can be viewed in the online issue, which is available at wileyonlinelibrary.com.]

using two circular disc specimens with a diameter of 10mm and a thickness of 3mm in shear mode at room temperature.

RESULTS AND DISCUSSION

Verification of MRE Damping Capacity

A preliminary assessment of the validity of the model was carried out by conducting an experiment using isotropic and anisotropic MREs. The dependency of frequency, strain amplitude, iron sand content and magnetic field on MRE damping capacity was investigated and the relationship between the theoretical model and experimental results assessed.

Viscous Damping. As shown in eq. (6), viscous damping (ψ_V) is frequency dependent. For assessing the validity of the viscous damping, unfilled natural rubber sample was prepared to rule out the influence of interfacial damping and magnetism induced damping and tan δ was measured through DMA over a range of

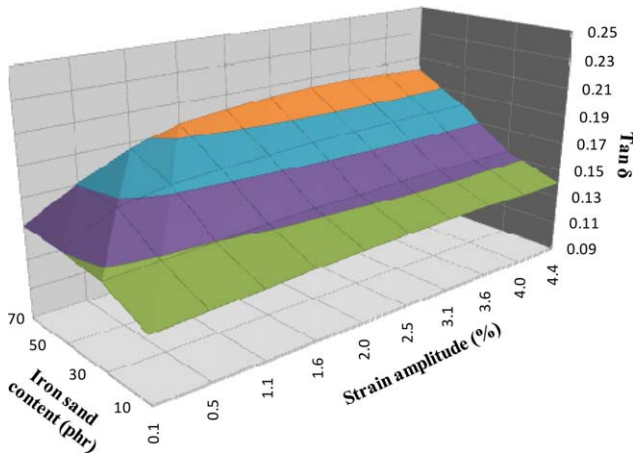

Figure 7. Influence of iron sand content and strain amplitude on tan δ. [Color figure can be viewed in the online issue, which is available at wileyonlinelibrary.com.]

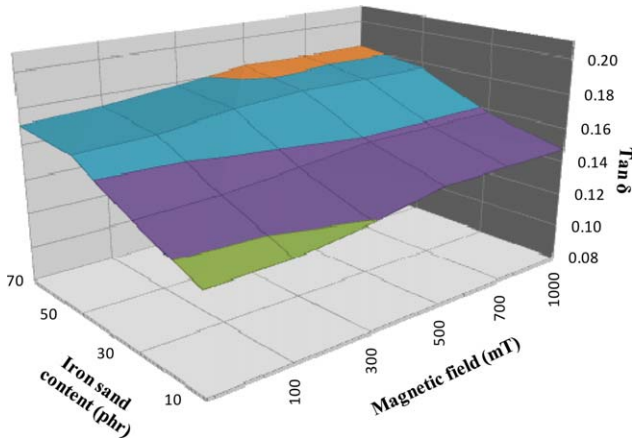

Figure 8. Influence of iron sand content and magnetic field on tan δ. [Color figure can be viewed in the online issue, which is available at wileyonlinelibrary.com.]

frequency (0.01–130 Hz) and strain amplitude (0.1%-4.5). The results are shown in Figure 6. Tan δ increased with increasing frequency and remained constant as the strain amplitude increased, supporting the proposed model for viscous damping. This trend was also in general agreement with other researchers.[42]

Interfacial Damping. As represented in eq. (19), interfacial damping is related to the particle content and applied strain amplitude. For assessing the validity of this equation, a series of isotropic MREs containing different contents of silane modified iron sand (10, 30, 50, and 70 phr) was prepared such that giving strongly bonded interfaces (although it is accepted that weakly bound interfacial area is likely to also be present for partially bonded iron sand) and curing was carried out in the absence of a magnetic field in order to rule out the influence of magnetism induced damping. Tan δ was measured over a range of strain amplitude (0.1%-4.5) and the results are shown in Figure 7. Generally, tan δ increased with the increased content of iron sand as well as the strain amplitude. As can also be seen, at lower iron sand contents (10 and 30 phr), tan δ showed slight increases over the whole strain amplitude range explored,

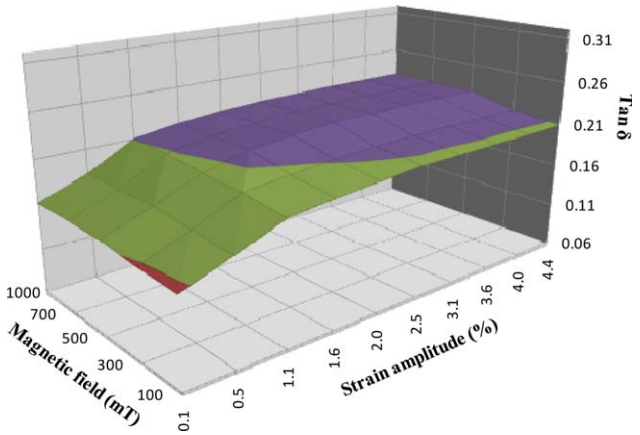

Figure 9. Influence of magnetic field and strain amplitude on tan δ. [Color figure can be viewed in the online issue, which is available at wileyonlinelibrary.com.]

Table II. Comparison of Theoretical Damping Capacity (ψ_{MRE}) with Tan δ Obtained from Experiments for MREs Containing Different Contents of Modified Iron Sand in a Rubber Matrix and Tested at Different Frequencies, Strain Amplitudes, and Magnetic Fields

Factor						
Iron sand content (phr)	Frequency (Hz)	Strain amplitude (%)	Magnetic field (mT)	Damping capacity, ψ_{MRE} of MREs according to proposed model	Experimental tan δ of MREs	Difference (%)
0	100	0.5	0	0.1689	0.1202	40.5
10	100	0.5	500	0.1741	0.1472	18.3
30	100	0.5	500	0.1832	0.1584	15.6
50	100	0.5	500	0.1916	0.1772	8.1
70	100	0.5	500	0.1993	0.1828	9.0
70	50	0.5	500	0.1148	0.1493	−23.1
70	120	0.5	500	0.2330	0.2182	6.7
70	100	1.5	500	0.2043	0.2175	−6.1
70	100	4.0	500	0.2107	0.2265	−7.0
70	100	0.5	100	0.1988	0.1731	14.9
70	100	0.5	300	0.1990	0.1778	11.9
70	100	0.5	1000	0.1993	0.1822	9.3
Average difference (%)						**8.1**

supporting that at low iron sand contents, energy absorption through viscous damping outweighs that through interfacial damping. At higher iron sand contents (50 and 70 phr), tan δ increased with increase in strain amplitude at low strain amplitudes and plateaued at higher strain amplitude. The amplitude dependence at low strain amplitudes for strongly bonded interfaces can be explained due to increased energy absorbed in bringing viscous flow of constrained materials at the particle interfaces and breakage of interfacial bonding; for weakly bonded interfaces increased energy could be absorbed due to breakdown of physical bonding/mechanical interlocking between iron sand and rubber and interfacial friction between iron sand and rubber. At the plateau region (above approximately 2.5% strain amplitude), all interactions are destroyed to such an extent they cannot be reconstructed and damping is largely relevant on the rubber matrix which and the friction between rubber chains and iron sand. Overall, an increase of tan δ with increased iron sand content as well as strain amplitude showed good agreement with the proposed model for interfacial damping (ψ_I).

Magnetism Induced Damping. As stated in eq. (25), magnetic induced damping of MREs is related to iron sand content, strain amplitude and magnetic field up to saturation magnetisation. For assessing the validity of the magnetic induced damping, a series of MRE samples containing different contents of silane modified iron sand (10, 30, 50 and 70 phr) was prepared and curing was carried out in the absence and presence of different magnetic fields (100, 300, 500, 700 and 1000 mT).

Table III. Comparison of Theoretical Damping Capacity (ψ_{MRE}) with Tan δ Obtained from Experiments for MREs Containing Different Contents of Unmodified Iron Sand in a Rubber Matrix and Tested at Different Frequencies, Strain Amplitudes, and Magnetic Fields

Factor						
Iron sand content (phr)	Frequency (Hz)	Strain amplitude (%)	Magnetic field (mT)	Damping capacity, ψ_{MRE} of MREs according to proposed model	Experimental tan δ of MREs	Difference (%)
30	100	0.5	700	0.1745	0.1101	58.5
70	100	0.5	0	0.1804	0.1348	33.8
70	50	0.5	300	0.0961	0.1076	−10.6
70	100	0.5	300	0.1806	0.1421	27.1
70	120	0.5	300	0.2143	0.1965	9.0
70	100	1.5	300	0.1857	0.1615	15.0
70	100	4.0	300	0.1921	0.1605	19.7
Average difference (%)						**21.8**

Table V. Average Percentage Contribution of ψ_V, ψ_I and ψ_M to the Total Damping ψ_{MRE} for MREs Containing Different Contents of Unmodified Iron Sand in a Rubber Matri

Factor				Damping capacity, ψ				Percentage contribution (%)		
Iron sand content (phr)	Frequency (Hz)	Strain amplitude (%)	Magnetic field (mT)	ψ_V	ψ_I	ψ_M	ψ_{MRE}	ψ_V	ψ_I	ψ_M
30	100	0.5	700	0.1689	0.00543	0.00021	0.1745	96.77	3.11	0.12
70	100	0.5	0	0.1689	0.01153	0.00000	0.1804	93.61	6.39	0.00
70	50	0.5	300	0.0844	0.01153	0.00016	0.0961	87.83	12.00	0.17
70	100	0.5	300	0.1689	0.01153	0.00016	0.1806	93.52	6.39	0.09
70	120	0.5	300	0.2026	0.01153	0.00016	0.2143	94.54	5.38	0.08
70	100	1.5	300	0.1689	0.01664	0.00020	0.1857	90.93	8.96	0.11
70	100	4.0	300	0.1689	0.02307	0.00020	0.1921	87.89	12.01	0.11
Average percentage contribution (%)								**92.16**	**7.75**	**0.10**

Figure 8 shows the variation of tan δ with iron sand content and magnetic field which was measured at a fixed frequency (100Hz) and strain amplitude (0.5%). It can be seen that tan δ increased with increased content of iron sand as well as increasing magnetic field. The increase of tan δ with increasing iron sand content can be explained by the increase in energy losses caused by interfacial damping with increase in iron sand content; furthermore for anisotropic MREs, increased energy could be absorbed through magnetism induced damping. As can also be seen, there is generally a slight increase in tan δ with increased magnetic field which levels off at about 500 mT, supporting saturation magnetization to be occurring at around 500 mT.

Figure 9 shows the variation of tan δ with magnetic field and strain amplitude which was measured using MRE sample containing fixed silane modified iron sand (70 phr). It can be seen that tan δ increased with increasing magnetic field at most strain amplitudes and then leveled off at around 500 mT due to saturation magnetization. It is also apparent that tan δ increased with increase in strain amplitude at low strain amplitudes and plateaued at higher strain amplitude. The amplitude dependence at low strain amplitudes could again be explained due to increase energy absorbed through interfacial damping. For anisotropic MREs, similar mechanisms would be involved as well as further energy absorbed through magnetism induced damping. At the plateau region, tan δ is largely reliant on the rubber matrix as previous explained in "Interfacial Damping" section. Overall, the obtained data for the influence of iron sand content, strain amplitude and magnetic field on tan δ supports proposed model for magnetic induced damping (ψ_M).

Table IV. Average Percentage Contribution of ψ_V, ψ_I and ψ_M to the Total Damping ψ_{MRE} for MREs Containing Different Contents of Modified Iron Sand in a Rubber Matrix

Factor				Damping capacity, ψ				Percentage contribution (%)		
Iron sand content (phr)	Frequency (Hz)	Strain amplitude (%)	Magnetic field (mT)	ψ_V	ψ_I	ψ_M	ψ_{MRE}	ψ_V	ψ_I	ψ_M
0	100	0.5	0	0.1689	0.00000	0.00000	0.1689	100.00	0.00	0.00
10	100	0.5	500	0.1689	0.00483	0.00045	0.1741	96.97	2.77	0.26
30	100	0.5	500	0.1689	0.01389	0.00045	0.1832	92.17	7.58	0.25
50	100	0.5	500	0.1689	0.02224	0.00045	0.1916	88.15	11.61	0.24
70	100	0.5	500	0.1689	0.02995	0.00045	0.1993	84.74	15.03	0.23
70	50	0.5	500	0.0844	0.02995	0.00045	0.1148	73.52	26.08	0.39
70	120	0.5	500	0.2026	0.02995	0.00045	0.2330	86.95	12.85	0.19
70	100	1.5	500	0.1689	0.03503	0.00045	0.2043	82.64	17.14	0.22
70	100	4.0	500	0.1689	0.04143	0.00045	0.2107	80.13	19.66	0.21
70	100	0.5	100	0.1689	0.02995	0.00002	0.1988	84.93	15.06	0.01
70	100	0.5	300	0.1689	0.02995	0.00016	0.1990	84.87	15.05	0.08
70	100	0.5	1000	0.1689	0.02995	0.00045	0.1993	84.74	15.03	0.23
Average percentage contribution (%)								**87.05**	**12.76**	**0.18**

Comparison between Tan Δ With Theoretical ψ_{MRE}. Comparison between tan δ with ψ_{MRE} was carried out on a series of isotropic and anisotropic MREs. ψ_{MRE} for MREs with modified and unmodified iron sand was calculated using eqs. (26) and (27), respectively. The results are shown in Tables II and III. Generally, ψ_{MRE} increases with increased in frequency, strain amplitude, iron sand content and magnetic field up to magnetic saturation and the trend matches the experimental trend; the values were generally higher than for tan δ with average percentage differences for modified and unmodified iron sand of 8.1% and 21.8%, respectively. Tables IV and V show the average percentage contribution of ψ_V, ψ_I and ψ_M to the total damping (ψ_{MRE}) or MREs containing different content of modified and unmodified iron sand in a rubber matrix. ψ_V was found to be the highest for MREs with modified and unmodified iron sand suggesting energy is mainly absorbed through the viscous flow of the rubber matrix. There also appears to be a higher ψ_I for MREs with modified iron sand compared with MREs with unmodified iron sand, supporting that the strongly bonded interfaces provide larger damping. In addition, it is possible to increase contributions of ψ_M to the total damping of MREs by testing the materials under an applied magnetic field in active or semi-active mode, however, further work would be needed to assess that.

The disparity of predicted damping capacity of MREs, ψ_{MRE} and experimental tan δ is not surprising when all the assumptions of the model (previously described separately in the sections for different mechanisms) are considered which are summarized as follows:

- $\psi_{MRE} \approx \tan\delta$ (although $\psi_V \approx tan\ \delta$ is accepted for viscous damping, this has not been previously shown to cover all mechanisms in MREs).
- The viscous damping of MREs follows the linear Kelvin Voight model. In reality, however, nonlinearity could occur due to addition of iron sand particles in the rubber matrix would changes the viscoelastic characteristics of the rubber.
- Iron sand particles were assumed to be spherical with the same diameter, however, the particles were not perfectly spherical or having the same diameter due to the milling process during preparation of iron sand as previously discussed in "Materials" section.
- In magnetism induced damping, the energy absorbed through magnetomechanical damping was considered insignificant due to the energy losses due to change of the magnetic domain structure is very difficult to directly measured.
- The iron sand particles are assumed to be aligned in long chains, however, the particles were not perfectly aligned in long chains during curing process under an applied magnetic field as reported elsewhere.[25–27]

However, given the limitations of other models that cover all mechanisms for MREs, this model could potentially use to predict damping of MRE for different types of matrices and magnetic particles as well as provide a guideline to manufacture MREs with desired damping performance. It also gives support that the following approximation can be used to determine damping of MREs at various variable factors:

$$\psi_{MRE} \approx \tan\delta \tag{28}$$

CONCLUSIONS

A theoretical model was developed to determine the total damping capacity of MREs (ψ_{MRE}) from viscous flow of the rubber matrix, interfacial damping and magnetic induced damping. ψ_{MRE} was found to be dependent on frequency, iron sand content, strain amplitude and magnetic field up to magnetic saturation. An experiment was carried out to assess the proposed model and comparison between tan δ with ψ_{MRE} on a series of isotropic and anisotropic MREs showed that ψ_{MRE} matched the experimental trends for tan δ with average percentage difference of 8.1% and 21.8% for MREs with modified and unmodified iron sand, respectively. It is considered that the model can provide a guideline to manufacture MREs with desired damping performance.

ACKNOWLEDGMENTS

The authors thank for the support from the Polymer and Composite Research Group of the University of Waikato.

REFERENCES

1. Chen, L.; Gong, X. L.; Li, W. H. *Polym. Test.* **2008**, *27*, 340.
2. Chokkalingam, R.; Rajasabai Senthur, P.; Mahendran, M. *J. Compos. Mater.* **2010**, *45*, 1545.
3. Fuchs, A.; Zhang, Q.; Elkins, J.; Gordaninejad, F.; Evrensel, C. *J. Appl. Polym. Sci.* **2007**, *105*, 2497.
4. Ginder, J. *Proc. SPIE* **1999**, *3675*, 131.
5. Lerner, A. A.; Cunefare, K. A. *J. Intell. Mater. Syst. Struct.* **2008**, *19*, 551.
6. Sun, T. L.; Gong, X. L.; Jiang, W. Q.; Li, J. F.; Xu, Z. B.; Li, W. H. *Polym. Test.* **2008**, *27*, 520.
7. Wang, Y.; Hu, Y.; Deng, H.; Gong, X.; Zhang, P.; Jiang, W.; Chen, Z. *Polym. Eng. Sci.* **2006**, *46*, 264.
8. Deng, H. X.; Gong, X. L. *Commun. Nonlinear Sci. Numeric. Simul.* **2008**, *13*, 1938.
9. Dyke, S. J.; Spencer, J. R.; Sain, M. K.; Carlson, J. D. *Smart Mater. Struct.* **1996**, *5*, 565.
10. Popp, K. M.; Kroger, M.; Li, W.; Zhang, X. Z.; Kosasih, P. B. *J. Intell. Mater. Syst. Struct.* **2010**, *21*, 1471.
11. Zhou, X.; Sun, Y.; Jiang, Y.; Liu, Y.; Zhao, G. *Polym. Bull.* **2011**, *66*, 1281.
12. Stepanov, G. V.; Abramchuk, S. S.; Grishin, D. A.; Nikitin, L. V.; Kramarenko, E. Y.; Khokhlov, A. R. *Polymer* **2007**, *48*, 488.
13. Collette, C.; Kroll, G.; Saive, G.; Guillemier, V.; Avraam, M.; Preumont, A. *J. Phys. Conf. Ser.* **2009**, *149*, 012091.
14. Nayak, B.; Dwivedy, S. K.; Murthy, K. S. R. K. *J. Sound Vib.* **2010**, *330*, 1837.
15. Gong, X. L.; Zhang, X. Z.; Zhang, P. Q. *Polym. Test.* **2005**, *24*, 669.
16. Davis, L. C. *J. Appl. Phys.* **1999**, *85*, 3348.
17. Jolly, M. R.; Carlson, J. D. B. C. M. *Smart Mater. Struct.* **1996**, *5*, 607.

18. Lin, C.; Xing-long, G.; Wei-hua, L. *Chin. J. Chem. Phys.* **2008**, *21*, 581.
19. Yanceng, F.; Xinglong, G.; Shouhu, X.; Wei, Z.; Jian, Z.; Wanquan, J. *Smart Mater. Struct.* **2011**, *20*, 1.
20. Chen, L.; Jerrams, S. *J. Appl. Phys.* **2011**, *110*, 013513.
21. Jie, Y.; Xinglong, G.; Huaxia, D.; Lijun, Q.; Shouhu, X. *Smart Mater. Struct.* **2012**, *21*, 125015.
22. Kelly, A.; Tyson, a. W. R. *J. Mech. Phys. Solids* **1965**, *13*, 329.
23. Eshelby, J. D. *Solid State Phys.* **1956**, *3*, 79.
24. Popov, V. L. In Contact Mechanics and Friction; Springer: Berlin, **2010**.
25. Raa Khimi, S.; Pickering, K. L. *Compos. Part B: Eng.* **2015**, *83*, 175.
26. Pickering, K. L.; Raa Khimi, S.; Ilanko, S. *Compos. Part A: Appl. Sci. Manuf.* **2015**, *68*, 377.
27. Raa Khimi, S.; Pickering, K. L.; Mace, B. R. *J. Appl. Polym. Sci.* **2015**, *132*, 41506.
28. De Silva, C. W. Vibration Damping, Control, and Design; CRC Press: Florida: **2007**.
29. Schoeck, G. *Phys. Stat. Solid (B)* **1969**, *32*, 651.
30. Lavernia, E. J.; Perez, R. J.; Zhang, J. *Metal. Mater. Trans. A* **1995**, *26*, 2803.
31. Graesser, E. J.; Wong, C. R. Symposium on M3D: Mechanics and Mechanisms of Material Damping, VK Kinra, and A. Wolfenden, Eds., American Society for Testing Materials; Philadelphia, **1992**, p 316.
32. Lakes, R. S. *J. Compos. Mater.* **2001**, *36*, 287.
33. Radiguet, M.; Kammer, D. S.; Molinari, J. F. *Mechan. Mater.* **2014**, *80*, 276.
34. Buyukozturk, O.; Nilson, A. H.; Slate, F. O. *J. Eng. Mech. Div.* **1972**, *98*, 581.
35. McKnight, G. P.; Carman, G. P. Materials Research Symposium; Smart Materials: Boston, USA, **1999**.
36. Geoffrey, P. M.; Gregory, P. C. Energy Absorption in Axial and Shear Loading of Particulate Magnetostrictive Composites. In: Christopher SL, Ed. Smart Structures and Materials 2000: Active Materials: Behavior and Mechanics; SPIE: Newport Beach, CA, **2000**; p 572.
37. Choudhury, P. K.; Singh, O. N. In Encyclopedia of RF and Microwave Engineering; John Wiley & Sons, Inc.: New Jersey, United States, **2005**.
38. Kallio, M. The Elastic and Damping Properties of Magnetorheological Elastomers; VTT Technical Research Centre of Finland: Finland, **2005**.
39. Chikazumi, S.; Graham, C. D. Physics of Ferromagnetism; Oxford University Press: New York, **1997**.
40. Schon, J. *Tribol. Int.* **2004**, *37*, 395.
41. Raa Khimi, S.; Pickering, K. L. *J. Appl. Polym. Sci.* **2013**, *131*, DOI: 10.1002/app.40008.
42. Rendek, M.; Lion, A. *Int. J. Solid. Struct.* **2010**, *47*, 2918.